World Journal of Advanced Research and Reviews
eISSN: 2581-9615 CODEN (USA): WJARAI
Cross Ref DOI: 10.30574/wjarr
Journal homepage: https://wjarr.com/

(RESEARCH ARTICLE)

Threshold-Induced Bifurcation and Chaos in a One-Dimensional Coastal Risk Adaptation Map

Hafidh Khoerul Fata *

Department of Mathematics, Universitas Diponegoro, Semarang, Indonesia.

World Journal of Advanced Research and Reviews, 2026, 30(03), 912-923

Publication history: Received on 08 May 2026; revised on 12 June 2026; accepted on 15 June 2026

Article DOI: https://doi.org/10.30574/wjarr.2026.30.3.1687

Abstract

Coastal disaster risk is often shaped by threshold mechanisms, where mitigation actions are activated after residual risk exceeds a critical level. This study proposes a one-dimensional threshold adaptation map for describing the evolution of normalized residual coastal risk under hazard amplification and adaptive response. The model combines logistic-type risk growth with a smooth sigmoidal threshold function representing the gradual activation of mitigation measures. Analytical results are obtained for the invariant interval, fixed points, local stability, and bifurcation conditions. The analysis shows that the sharpness of the threshold response plays a central role in determining the stability of the positive equilibrium. Numerical simulations using bifurcation diagrams, cobweb plots, time series, and Lyapunov exponents reveal period-doubling cascades and chaotic dynamics when the hazard amplification or threshold sharpness increases. These results indicate that adaptation may reduce residual risk when implemented gradually, but excessively abrupt threshold responses may generate persistent oscillations and chaotic fluctuations. The proposed model provides a simple mathematical framework for understanding threshold-induced instability in coastal disaster risk dynamics and highlights the importance of designing adaptive interventions that are dynamically smooth as well as effective.

Keywords: Coastal risk; Threshold adaptation; Bifurcation; Chaos; One-dimensional map; Lyapunov exponent

1. Introduction

Coastal disaster risk is increasingly shaped by the interaction between long-term sea-level rise, extreme water levels, urban exposure, and vulnerability in low-lying coastal systems (1). Even moderate sea-level rise may strongly increase the frequency of coastal flood exceedances, so events that were formerly rare can become recurrent stressors for coastal communities(2). Recent reviews of coastal flood risk assessment also indicate that uncertainty remains high because hazard processes, exposure patterns, and modelling choices are often treated separately (3). This difficulty becomes more pronounced when high-tide flooding is driven by interacting sea-level components rather than by a single forcing process (4).

A second difficulty concerns the temporal structure of coastal hazards. Rainfall, storm surge, tide, and mean sea level may coincide in ways that amplify flood impacts beyond the effect of each driver alone (5). In Ho Chi Minh City, for example, ignoring the monthly variability and dependence between rainfall and sea levels was shown to underestimate expected annual damage substantially (6). Integrated hydraulic models have been developed to represent compound flooding under climate change, but such models are usually designed for spatially detailed risk assessment rather than for isolating the nonlinear feedback mechanism behind stability loss(7). Hence, there remains value in reduced dynamical models that clarify how a small number of mechanisms can produce qualitative transitions in residual risk.

* Corresponding author: Hafidh Khoerul Fata

Adaptation studies have responded to these uncertainties by developing threshold-oriented planning concepts. Coastal flood management can be framed through adaptation tipping points, where an existing strategy ceases to satisfy its performance objective under changing environmental conditions (8). The broader adaptation tipping point approach shifts attention from a single projected future to the conditions under which a policy fails (9). Dynamic Adaptive Policy Pathways then arrange actions over time so that decision-makers can move from one strategy to another when monitored conditions justify a change (10). Trigger-based adaptation extends this logic by identifying signals that indicate when sea-level rise or flood frequency has reached a level requiring intervention (11). Recent infrastructure studies under deep uncertainty show that such pathways are useful when long-lived coastal assets must remain functional across multiple future scenarios (12). Multi-dimensional extensions of DAPP further show that interacting risks may alter the timing and effectiveness of adaptation choices (13).

However, a planning threshold is not the same as a dynamical threshold. Coastal adaptation frameworks usually identify when an intervention should be reconsidered, but they do not necessarily describe how the activation of that intervention modifies the trajectory of residual risk (10). Studies on estuarine adaptation emphasize that coastal systems require flexible responses to sea-level rise, yet the mathematical shape of the response function is rarely treated as a source of instability (14). Nature-based coastal protection can reduce exposure and support resilience, but its effect on long-term risk still depends on how the protective response is represented in the risk dynamics (15). This distinction is important because a strong intervention may not be dynamically benign if it is activated too abruptly near a critical threshold.

The mathematical motivation comes from one-dimensional discrete dynamical systems. Classical nonlinear maps show that a scalar recurrence can generate stable equilibria, periodic oscillations, and chaotic fluctuations without external randomness (16). The theorem that period three implies chaos established that simple interval maps may contain deterministic complexity once certain periodic structures are present (17). Feigenbaum's universality results further showed that period-doubling cascades follow robust scaling laws in broad classes of unimodal maps (18). Later work connected period-doubling cascades more explicitly with the emergence of chaotic dynamics in discrete systems (19,20). These results suggest that low-dimensional maps can be analytically simple while still capturing nontrivial transitions between stability, periodicity, and chaos.

For a one-dimensional map, the slope near an equilibrium is central to local stability. A fixed point is stable when the absolute value of the derivative is less than one, while loss of stability through a multiplier crossing minus one corresponds to a flip bifurcation (21). Lyapunov exponents provide a complementary diagnostic because they measure the average exponential rate of separation of nearby trajectories (22). The mathematical theory of Lyapunov exponents provides the basis for distinguishing regular and chaotic regimes in deterministic systems (23). Similar mechanisms are not only abstract; period-doubling and chaotic transitions have also been observed in simple ecological models, showing that low-dimensional nonlinear feedback may be relevant in applied settings(24).

These two lines of literature motivate the present study. Coastal adaptation research provides concepts of thresholds, triggers, and adaptive pathways, while one-dimensional dynamics provides tools for fixed-point stability, bifurcation, and Lyapunov analysis. What is still missing is a minimal discrete model that links these perspectives through the dynamics of residual coastal risk. This paper proposes a one-dimensional threshold adaptation map in which logistic-type risk amplification is multiplied by a smooth sigmoidal adaptive response. The model is used to examine whether adaptation that is intended to reduce residual risk can also generate oscillations or chaos when its activation around the threshold becomes too sharp.

The contribution of the paper is threefold. First, it formulates a bounded one-dimensional map for normalized residual coastal risk with explicit parameters for hazard amplification, adaptation effectiveness, activation threshold, and threshold sharpness. Second, it derives fixed-point, stability, and bifurcation conditions that identify how the slope of the adaptive response affects equilibrium stability. Third, it uses bifurcation diagrams, time series, cobweb plots, and Lyapunov exponents to show that both hazard amplification and threshold sharpness can induce period-doubling and chaotic dynamics. The resulting model is not intended to replace data-driven coastal flood models, but to provide a compact mathematical mechanism for understanding threshold-induced instability in adaptive coastal risk dynamics.

2. Literature review

Discrete-time models are often used when a process is observed step by step rather than continuously. In their simplest form, such models appear as one-dimensional maps, where the next state depends only on the present state. Although this structure looks elementary, it can already produce rich long-term behavior. The logistic map, for example, shows how a single nonlinear feedback term may lead from a stable equilibrium to periodic oscillations and eventually to chaos

through a sequence of period-doubling bifurcations (16,25). This classical result is useful beyond population dynamics. It reminds us that irregular behavior in an observed system does not always come from random disturbance; sometimes it is generated by the deterministic rule that governs the system itself.

This point is relevant for risk modelling. A risk indicator may fluctuate because of external forcing, but it may also fluctuate because the response mechanism is nonlinear. In coastal areas, risk is shaped by several interacting factors, including sea-level rise, storm surge, rainfall, land subsidence, exposure, and vulnerability. These factors do not always affect communities in a smooth or proportional way. A small increase in water level, for instance, may have limited impact when it remains below a critical elevation, but may produce serious damage once that level is exceeded. For this reason, threshold thinking has become an important part of coastal risk and climate adaptation studies (1,2).

Thresholds also appear in adaptation planning. The concept of adaptation tipping points describes situations in which an existing strategy is no longer able to meet its objectives under changing environmental conditions (9). This idea has influenced the development of dynamic adaptive policy pathways, where decisions are revised when certain signals, triggers, or limits are reached (10,26). Such approaches are valuable because they recognize uncertainty and allow policies to change over time. Still, they are usually designed as planning frameworks, not as low-dimensional dynamical systems. As a result, they do not directly show how the mathematical shape of an adaptive response may affect stability.

A key issue is that adaptation is not only about how strong an intervention is. The way the intervention is activated also matters. A gradual response may reduce risk without creating large oscillations. By contrast, a very sharp response near a threshold can introduce a steep change in the feedback rule. From the viewpoint of one-dimensional dynamics, this steepness changes the slope of the map near the equilibrium. If the slope becomes too negative, a stable fixed point may lose stability through a flip bifurcation. After that, periodic and chaotic behavior may occur. In practical terms, an adaptation rule that is intended to stabilize residual risk may produce recurrent fluctuations when it acts too abruptly.

Most studies on one-dimensional chaotic maps focus on mathematical mechanisms, population models, or technical applications such as cryptography and signal processing. Meanwhile, coastal risk research is commonly developed through flood frequency analysis, exposure assessment, hydrodynamic modelling, or adaptation pathway planning. These two lines of work are both important, but they rarely meet in a minimal model that connects threshold-based adaptation with bifurcation and chaos in residual coastal risk. This study addresses that gap by proposing a one-dimensional threshold adaptation map. The model combines logistic-type risk growth with a sigmoidal adaptive response, allowing the sharpness of the threshold mechanism to be varied explicitly. Through this construction, the study examines whether mitigation that is designed to reduce risk may also become a source of instability when its activation around the threshold is too abrupt (6).

3. Methodology

This study develops a one-dimensional discrete model to describe the evolution of normalized residual coastal risk. The variable $x_n \in [0,1]$ denotes the level of residual risk at the n-th observation period. A value close to zero represents a low-risk condition, while a value close to one indicates a high accumulated risk. The proposed map is defined as

$$x_{n+1} = F(x_n) = r\, x_n(1 - x_n)[1 - \gamma\, S_m(x_n - \theta)] \tag{1}$$

The threshold response function is given by

$$S_m(x_n - \theta) = \frac{1}{1 + exp[-m(x_n - \theta)]} \tag{2}$$

In this model, the term $r\, x_n(1 - x_n)$ represents nonlinear risk amplification with a self-limiting effect. The parameter $r > 0$ measures the intensity of hazard amplification, which may be associated with increasing exposure, sea-level pressure, storm surge potential, rainfall intensity, or other external stressors. The multiplicative term $[1 - \gamma\, S_m(x_n - \theta)]$ represents the reduction of residual risk due to adaptation or mitigation. The parameter $\gamma \in [0,1)$ denotes adaptation effectiveness, $\theta \in (0,1)$ is the risk threshold at which adaptation begins to become active, and $m > 0$ controls the sharpness of the response near the threshold.

The sigmoidal function in equation (2) is used to represent a smooth threshold mechanism. When the residual risk is far below θ, the value of $S_m(x_n - \theta)$ is close to zero, so the adaptive reduction is weak and the system behaves close to a logistic-type risk growth model. When x_n approaches or exceeds θ, the threshold function increases and the adaptive

response become stronger. A small value of m produces a gradual response, while a large value of m makes the response more abrupt. This distinction is important because the model is intended to examine not only the strength of adaptation, but also how sharply adaptation is activated around the critical risk level.

The analytical part of the study begins by examining the boundedness of the model. Since x_n is interpreted as normalized residual risk, the interval [0,1] must remain dynamically meaningful. For $0 < r \leq 4, 0 \leq \gamma < 1$, and $x_0 \in [0,1]$, the orbit remains in [0,1]. This follows from the fact that $0 \leq x(1-x) \leq 1/4$ for $x \in [0,1]$, while $0 < 1 - \gamma S_m(x-\theta) \leq 1$. Therefore, the map sends normalized risk values into normalized risk values, and the model is consistent with its interpretation.

Fixed points are obtained by solving $F(x^*) = x^*$. The trivial fixed point is $x^* = 0$. A positive fixed point, when it exists, satisfies

$$1 = r(1-x^*)[1-\gamma S_m(x^*-\theta)]. \tag{3}$$

This positive fixed point represents a long-term residual risk level under the interaction between hazard amplification and adaptive reduction. Its stability is determined by the derivative of the map. The derivative of F is

$$F'(x) = r(1-2x)[1-\gamma S_m(x-\theta)] - r\gamma m x(1-x)S_m(x-\theta)[1-S_m(x-\theta)]. \tag{4}$$

A fixed point x^* is locally asymptotically stable if

$$|F'(x^*)| < 1. \tag{5}$$

Loss of stability is then examined through standard bifurcation conditions for one-dimensional maps. A fold bifurcation may occur when

$$F(x^*) = x^* \text{ and } F'(x^*) = 1, \tag{6}$$

while a flip bifurcation may occur when

$$F(x^*) = x^* \text{ and } F'(x^*) = -1. \tag{7}$$

The second term in equation (4) plays an important role in this model. This term depends directly on the threshold sharpness parameter m. As m increases, the adaptive response becomes steeper near the threshold, which may make the slope of the map more negative. Consequently, a threshold mechanism that is intended to reduce risk may also destabilize the positive fixed point if it is activated too abruptly.

Numerical simulations are conducted to support the analytical findings. Bifurcation diagrams are generated by varying the hazard amplification parameter r and the threshold sharpness parameter m. For each parameter value, the orbit is iterated for a sufficiently long transient period, and only the later iterates are plotted. This procedure allows stable fixed points, periodic cycles, and chaotic regimes to be visually identified.

The Lyapunov exponent is also computed to detect sensitive dependence on initial conditions. It is approximated by

$$\lambda \approx \left(\frac{1}{N}\right)\sum_{n=1}^{N} \log|F'(x_n)|, \tag{8}$$

where the summation is taken after discarding transient iterations. A negative Lyapunov exponent indicates convergence to a stable fixed point or periodic orbit, while a positive Lyapunov exponent indicates chaotic behavior. Time series and cobweb plots are also used to illustrate representative dynamical regimes, including stable convergence, periodic oscillation, and chaotic fluctuation.

Unless otherwise stated, the simulations use $x_0 = 0.37$ as the initial condition. Several additional initial conditions in [0,1] are also tested to ensure that the observed dynamics are not caused by a particular starting value. The parameter ranges are chosen within the normalized setting of the model: $0 < r \leq 4, 0 \leq \gamma < 1, 0 < \theta < 1$, and $m > 0$. These ranges keep the model bounded while allowing the interaction between hazard amplification and threshold-based adaptation to be observed.

4. Results and discussion

The numerical experiments are designed to isolate two sources of instability in the proposed map: hazard amplification and threshold sharpness. Unless otherwise stated, the simulations use γ = 0.40 and θ = 0.55. The parameter m is fixed at 30 for the r −sweep, while r is fixed at 3.70 for the m −sweep. The initial condition is x_0 = 0.37, and transient iterates are discarded before plotting asymptotic states.

Table 1 Numerical settings used in the bifurcation and orbit simulations

Parameter varied	Fixed parameters	Main transition	Diagnostic
r	$\gamma = 0.40$, $\theta = 0.55$, $m = 30$	stable equilibrium →period doubling→ chaos	bifurcation diagram and Lyapunov exponent
m	$r = 3.70$, $\gamma = 0.40$, $\theta = 0.55$	smooth response → oscillatory and chaotic regimes	bifurcation diagram and Lyapunov exponent
$r = 2.00, 2.50, 3.70$	$\gamma = 0.40$, $\theta = 0.55$, $m = 30$	representative stable, periodic, and chaotic orbits	time series and cobweb plots
x_0	0.37	transient discarded before plotting	asymptotic orbit sampling

4.1. Threshold response and bounded dynamics

Let $A_m(x) = 1 - \gamma S_m(x - \theta)$ denote the adaptive multiplier. This factor separates the strength of adaptation, measured by , from the sharpness of its activation, measured by m. For the baseline value $\gamma = 0.40$, the lower limiting multiplier is $1 - \gamma = 0.60$, while $A_m(\theta) = 1 - \frac{\gamma}{2} = 0.80$. Thus increasing m does not change the eventual reduction level; it changes how abruptly the intervention is activated around the threshold.

$$A_m(x) = 1 - \gamma S_m(x - \theta), \quad A_m(\theta) = 1 - \frac{\gamma}{2}, \quad A'_m(\theta) = \frac{\gamma m}{4} \tag{9}$$

Equation (9) identifies the main mechanism of the model. The slope at the threshold is proportional to $-m$, so a large threshold sharpness produces a nearly switch-like response. Figure 1 shows this transition. For small m, the multiplier changes gradually across the interval. For large m, the curve is almost flat below and above theta, but steep near the threshold.

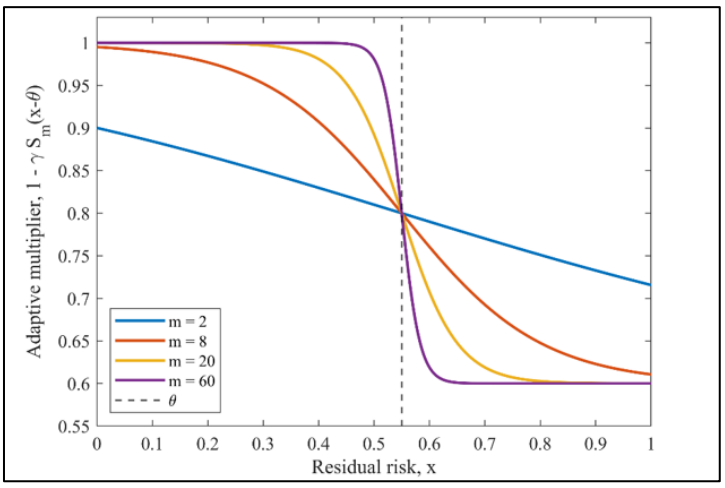

Figure 1 Smooth threshold response for $\gamma = 0.40$ and $\theta = 0.55$ under different values of m.

The map is dynamically meaningful on the normalized interval. Since $0 \leq x(1-x) \leq \frac{1}{4}$ for $x \in [0,1]$ and $0 < A_m(x) \leq 1$, one obtains

$$0 \leq F(x) = rx(1-x)A_m(x) \leq \frac{r}{4} \leq 1, \quad 0 < r \leq 4\,. \tag{10}$$

Hence $F([0,1])$ is contained in $[0,1]$ for the parameter range used in the simulations. This invariance is essential because x_n is interpreted as normalized residual coastal risk.

4.2. Equilibrium stability and bifurcation with respect to hazard amplification

The trivial equilibrium $x^* = 0$ always exists. A positive equilibrium satisfies

$$1 = r(1-x^*)A_m(x^*). \tag{11}$$

Its local stability is governed by the multiplier $F'(x^*)$. The equilibrium is locally asymptotically stable when $|F'(x^*)| < 1$. A flip bifurcation occurs when the multiplier passes through -1, that is, when eq. (7) satisfied.

For $\gamma = 0.40$, $\theta = 0.55$, and $m = 30$, the positive equilibrium loses stability at approximately $r = 2.1687$ with $x^* = 0.5013$. Below this value the orbit converges to a steady residual-risk level. As r increases, the stable equilibrium is replaced by periodic cycles and then by chaotic bands. The transition is visible in Figure 2. The Lyapunov exponent in Figure 3 supports this interpretation. Negative values correspond to stable fixed points or periodic orbits. Positive values indicate sensitive dependence on initial conditions. The positive intervals in the high-r region coincide with the dense bands in the bifurcation diagram. Periodic windows remain embedded in the chaotic region, which is typical for one-dimensional maps with folding.

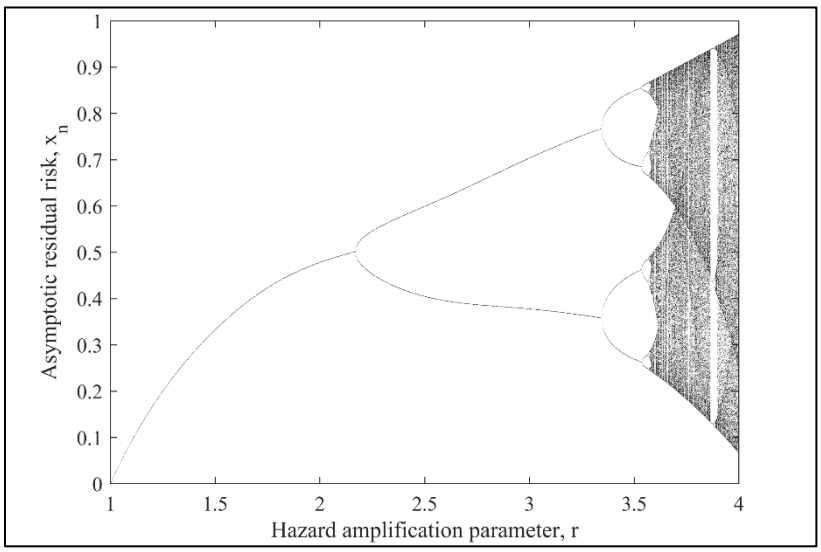

Figure 2 Bifurcation diagram with respect to the hazard amplification parameter r for $\boldsymbol{\gamma = 0.40}$, $\boldsymbol{\theta = 0.55}$, and $\boldsymbol{m = 30}$.

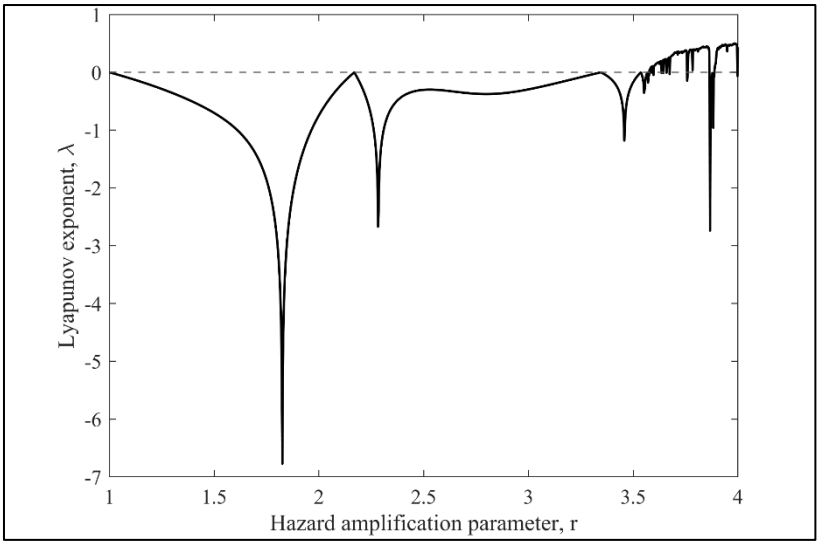

Figure 3 Lyapunov exponent corresponding to the $\boldsymbol{r}$-bifurcation diagram in Figure 2

4.3. Threshold sharpness as an independent route to instability

The most relevant feature of the proposed model is that complex dynamics can also be produced by increasing the sharpness of adaptation. This is not a change in hazard magnitude. It is a change in the form of the response rule. For fixed $r = 3.70, \gamma = 0.40, and\ \theta = 0.55$, Figure 4 shows that the asymptotic orbit changes considerably as m varies.

The destabilizing role of m is already present in the derivative of the map. The second term in $F'(x)$ is

$$-r\,\gamma\,m\,x(1-x)S_m(x-\theta)[1-S_m(x-\theta)]. \tag{12}$$

Near the threshold, this term scales approximately as $-r\,\gamma\,m\frac{x(1-x)}{4}$. It therefore steepens the map as m increases. A policy response that is intended to reduce residual risk may consequently make the return map locally too steep, which allows a stable residual-risk level to lose stability.

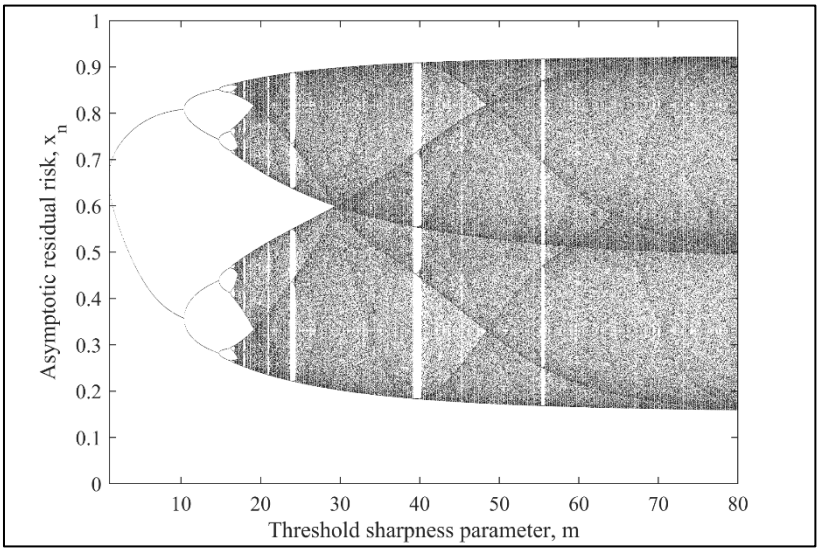

Figure 4 Bifurcation diagram with respect to the threshold sharpness parameter $\boldsymbol{m}$ for $\boldsymbol{r = 3.70, \gamma = 0.40}$, and $\boldsymbol{\theta = 0.55}$

The Lyapunov exponent in Figure 5 confirms that threshold sharpness is not merely a visual parameter. The exponent becomes positive after the onset of chaotic bands, with narrow negative windows corresponding to periodic regimes.

In the present parameter set, the first positive Lyapunov interval appears around $m = 16.8$, and chaotic behavior becomes dominant for larger m, although periodic windows persist.

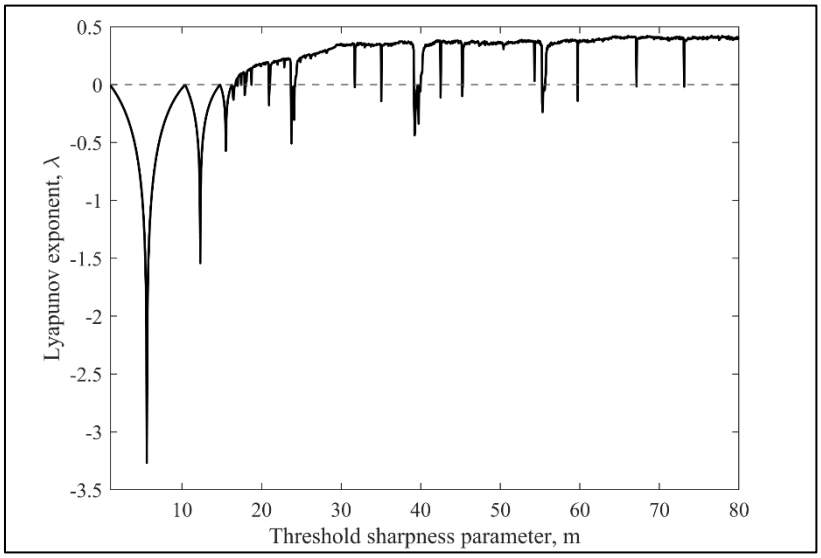

Figure 5 Lyapunov exponent corresponding to the $\boldsymbol{m}$ −bifurcation diagram in Figure 4

4.4. Representative time series and cobweb structures

Three representative regimes are shown in Figures 6(a)-(c). At $r = 2.00$, the orbit converges to a stable fixed point. At $r = 2.50$, the long-term behavior is a period-two oscillation, with residual risk alternating between two levels. At $r = 3.70$, the orbit fluctuates irregularly over a wider interval. These time series give a direct interpretation of the bifurcation diagrams: stable adaptation corresponds to a nearly constant risk level, periodic dynamics correspond to recurrent over- and under-correction, while chaos corresponds to irregular residual-risk fluctuations.

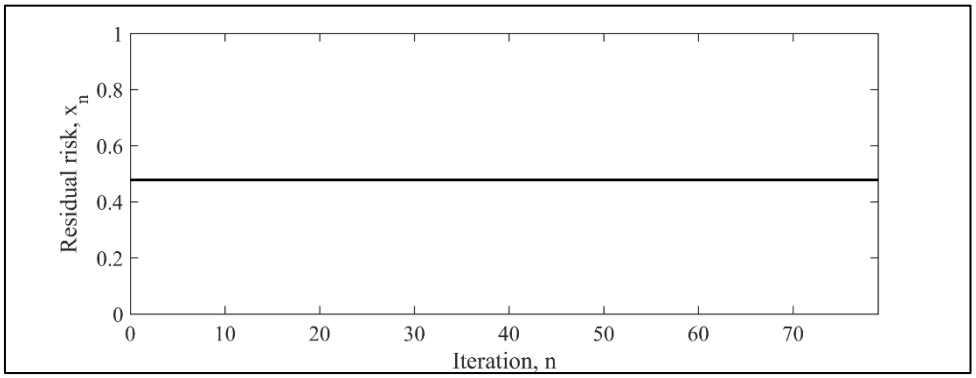

(***a***)

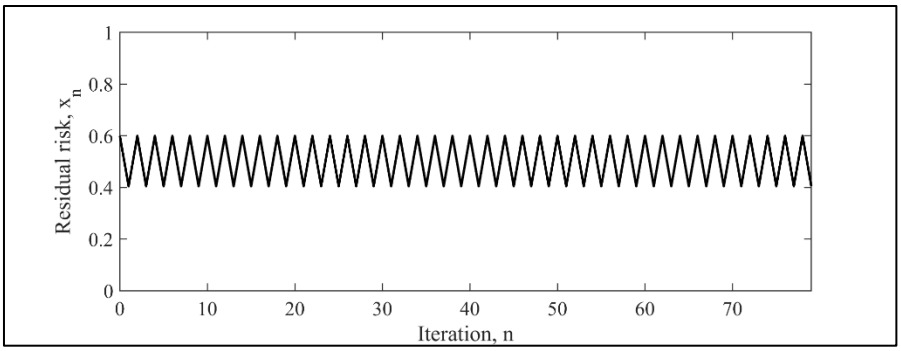

(***b***)

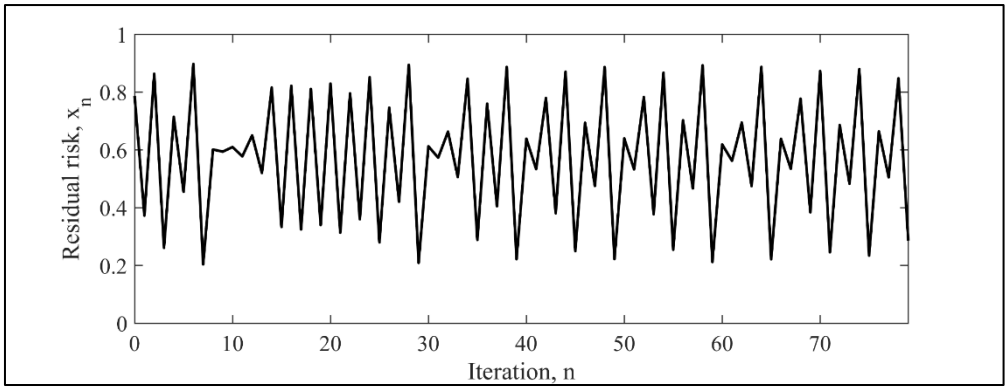

(c)

Figure 6 Time series for a chaotic fluctuation at $(\boldsymbol{a})\ \boldsymbol{r = 2.00}$, $(\boldsymbol{b})\ \boldsymbol{r = 2.50}$, $(\boldsymbol{c})\ \boldsymbol{r = 3.70}$, with $\boldsymbol{\gamma = 0.40}$, $\boldsymbol{\theta = 0.55}$, $\boldsymbol{and\ m = 30}$

The corresponding cobweb plots in Figure 7 clarify the geometry of the iteration. In the stable case, the cobweb converges to the intersection of $F(x)$ and the diagonal. In the periodic case, the path forms a rectangle, indicating a two-cycle. In the chaotic case, the path repeatedly crosses wide portions of the graph, showing the stretching and folding mechanism responsible for irregular dynamics.

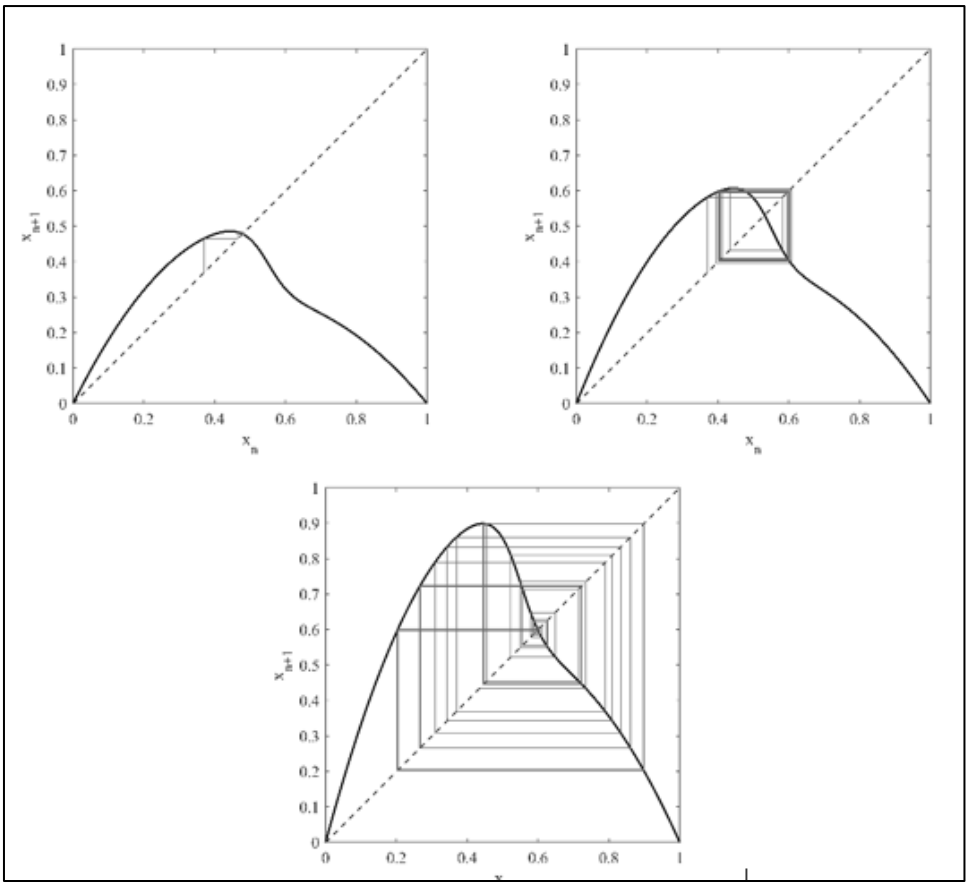

Figure 7 Cobweb plots for (left) stable fixed-point convergence, (center) period-two oscillation, and (right) chaotic fluctuation

4.5. Dynamic interpretation for coastal risk adaptation

The simulations identify two distinct routes to complex residual-risk dynamics. The first route is hazard amplification: increasing r raises the intrinsic pressure in the system and eventually destroys the stability of the positive equilibrium.

The second route is threshold sharpening: even when the hazard level is fixed, a sufficiently abrupt adaptive response can induce bifurcation and chaos. This distinction is important for adaptation design. A strong intervention is not necessarily destabilizing if it is activated smoothly. Conversely, a moderate intervention may destabilize the system if its activation is too abrupt near the threshold. In the language of the model, gamma controls the depth of risk reduction, while m controls the slope of the feedback. The latter can be as important as the former. The model should be interpreted as a minimal dynamical mechanism rather than a direct forecasting tool. It does not estimate real coastal losses or prescribe a specific engineering policy. Its contribution is qualitative: threshold-based adaptation can reduce residual risk, but it can also create persistent oscillations or chaotic fluctuations when the response rule is too sharp.

5. Conclusion

This study introduced a one-dimensional threshold adaptation map for normalized residual coastal risk. The map combines logistic-type risk amplification with a sigmoidal adaptive multiplier. The formulation keeps the dynamics in the normalized interval [0,1] for $0 < r \leq 4$, making the state variable consistent with its interpretation as residual risk.

Analytically, the positive equilibrium satisfies $1 = r(1 - x^*)A_m(x^*)$, and its local stability is determined by $|F'(x^*)| < 1$. The derivative shows explicitly how the sharpness parameter m enters the stability mechanism. In particular, the threshold term contributes a negative component to the slope of the map. This component becomes stronger when adaptation is activated more abruptly near the threshold.

Numerically, the model displays stable equilibria, period-two oscillations, period-doubling structures, periodic windows, and chaotic bands. Increasing r produces the expected transition from stability to complex dynamics. More importantly, increasing m can also generate bifurcation and chaos even when r is fixed. This result supports the central conclusion of the study: the dynamic smoothness of adaptation is as important as its effectiveness.

For coastal risk interpretation, the findings suggest that threshold-based intervention should not be evaluated only by how much risk it reduces. The way the intervention is activated also matters. A gradual response may stabilize residual risk, while an abrupt response can generate recurrent or irregular risk fluctuations.

Recommendations

Future work should calibrate the proposed map using empirical indicators of coastal residual risk, such as flood frequency, inundation duration, exposure index, or normalized damage records. Such calibration would allow the parameters $r, \gamma, \theta, and\ m$ to be interpreted more quantitatively for a specific coastal region. The next natural extension is to include seasonal forcing. Coastal hazards are often affected by seasonal rainfall, tides, and storm surge patterns. A non-autonomous version of the map with periodically varying r or θ could test whether seasonal pressure amplifies or suppresses threshold-induced instability. The model can also be extended to include uncertainty and spatial interaction. Stochastic perturbations would represent random extreme events, while coupled maps could describe multiple coastal communities or zones connected by hydrological, economic, or evacuation links. From a policy perspective, the model suggests that adaptation planning should consider response smoothness in addition to response strength. Trigger-based policies may be necessary, but their activation should be designed to avoid excessive overcorrection near the threshold. This provides a mathematical argument for adaptive interventions that are gradual, monitored, and adjustable over time.

Compliance with ethical standards

Disclosure of conflict of interest

No conflict of interest to be disclosed.

References

[1] Oppenheimer M, Glavovic BC, Hinkel J, van de Wal R, Magnan AK, Abd-Elgawad A, et al. Sea Level Rise and Implications for Low-Lying Islands, Coasts and Communities. In: Pörtner HO, Roberts DC, Masson-Delmotte V, Zhai P, Tignor M, Poloczanska E, et al., editors. IPCC Special Report on the Ocean and Cryosphere in a Changing Climate [Internet]. Cambridge, UK and New York, NY, USA: Cambridge University Press; 2019. p. 321–445.

Available from: https://www.ipcc.ch/srocc/chapter/chapter-4-sea-level-rise-and-implications-for-low-lying-islands-coasts-and-communities/

[2] Taherkhani M, Vitousek S, Barnard PL, Frazer N, Anderson TR, Fletcher CH. Sea-level rise exponentially increases coastal flood frequency. Sci Rep [Internet]. 2020;10(1):6466. Available from: https://doi.org/10.1038/s41598-020-62188-4

[3] Liu P, Din AHM, Hamden MH, Affandi MLA. Advancing coastal flood risk assessment: a systematic review of global research trends, hazard processes, modelling approaches, and key uncertainties. Environ Res Commun. 2026;

[4] Li S, Wahl T, Piecuch C, Dangendorf S, Thompson P, Enriquez A, et al. Compounding of sea-level processes during high-tide flooding along the U.S. coastline. J Geophys Res Ocean. 2023;128.

[5] Camus P, Haigh ID, Wahl T, Nasr AA, Mendez FJ, Darby SE, et al. Daily synoptic conditions associated with occurrences of compound events in estuaries along North Atlantic coastlines. Int J Climatol. 2022;

[6] Couasnon A, Scussolini P, Tran TVT, Eilander D, Muis S, Wang H, et al. A flood risk framework capturing the seasonality of and dependence between rainfall and sea levels: an application to Ho Chi Minh City, Vietnam. Water Resour Res [Internet]. 2022 Feb;58(2):1–19. Available from: https://www.scopus.com/pages/publications/85125148394

[7] Pasquier U, He Y, Hooton S, Hiscock KM. An integrated 1D-2D hydraulic modelling approach to assess the sensitivity of a coastal region to compound flooding hazard under climate change. Nat Hazards. 2019;

[8] Ramm TD, Watson CS, White CJ. Strategic adaptation pathway planning to manage sea-level rise and changing coastal flood risk. Environ Sci Policy. 2018;

[9] Kwadijk JCJ, Haasnoot M, Mulder JPM, Hoogvliet MMC, Jeuken ABM, van der Krogt RAA, et al. Using adaptation tipping points to prepare for climate change and sea level rise: a case study in the Netherlands. WIREs Clim Chang [Internet]. 2010 Sep 1;1(5):729–40. Available from: https://doi.org/10.1002/wcc.64

[10] Haasnoot M, Kwakkel JH, Walker WE, ter Maat J. Dynamic adaptive policy pathways: a new method for crafting robust decisions for a deeply uncertain world. Glob Environ Chang. 2013;23(2):485–98.

[11] Stephens SA, Bell RG, Lawrence J. Developing signals to trigger adaptation to sea-level rise. Environ Res Lett. 2018;13(10):104004.

[12] Allison AEF, Lawrence JH, Stephens SA, Stroombergen A. Planning for wastewater infrastructure adaptation under deep uncertainty. Front Clim. 2024;

[13] Curran PH, Johnson DR, Logan TM. DAPP-MD: a multi-dimensional framework for adaptive planning under deep uncertainty and interacting risks. Environ Sci Policy. 2026;

[14] Hinkel J, Schuerch M, French J, Nicholls RJ. Sea-Level Rise Risk and Adaptation in Estuaries. In: Climate Change and Estuaries. 2023.

[15] Manes S, Gama-Maia D, Vaz S, Bastos M, de Andrade FM, Vernier L, et al. Nature as a solution for shoreline protection against coastal risks associated with ongoing sea-level rise. Ocean Coast Manag. 2023;235:106487.

[16] May RM. Simple mathematical models with very complicated dynamics. Nature [Internet]. 1976;261(5560):459–67. Available from: https://doi.org/10.1038/261459a0

[17] Li TY, Yorke JA. Period three implies chaos. Am Math Mon. 1975;82(10):985–92.

[18] Feigenbaum MJ. Quantitative universality for a class of nonlinear transformations. J Stat Phys. 1978;19(1):25–52.

[19] Fata HK, Ashar NY. Bifurcations, Hidden Attractors, and Chaos in a Nonlinear Three-Dimensional System. Eur J Pure Appl Math [Internet]. 2025 Nov 5;18(4):6968. Available from: https://doi.org/10.29020/nybg.ejpam.v18i4.6968

[20] Sander E, Yorke JA. Connecting period-doubling cascades to chaos. Int J Bifurc Chaos. 2012;22(2):1250022.

[21] Luo ACJ. On bifurcations and local stability in 1-D nonlinear discrete dynamical systems. Int J Dyn Control. 2021;

[22] Skokos C. The Lyapunov characteristic exponents and their computation. In: Dynamics of Small Solar System Bodies and Exoplanets. Springer; 2010. p. 63–135.

[23] Young LS. Mathematical theory of Lyapunov exponents. J Phys A Math Theor. 2013;46(25):254001.

[24] Stone L. Period-doubling reversals and chaos in simple ecological models. Nature. 1993;365(6447):617–20.

[25] Devaney R. An Introduction To Chaotic Dynamical Systems [Internet]. CRC Press; 2018. (Advances in Mathematics and Engineering). Available from: https://books.google.co.id/books?id=8nhQDwAAQBAJ

[26] Stephens SA, Bell RG, Lawrence J. Developing signals to trigger adaptation to sea-level rise [Internet]. 2021. Available from: https://openaccess.wgtn.ac.nz/articles/journal_contribution/Developing_signals_to_trigger_adaptation_to_sea-level_rise/14349302